THE JOURNAL OF PHYSICAL CHEMISTRY A

Article

pubs.acs.org/JPCA

Conformation and Hydrogen-Bond-Assisted Polymerization in Glycine Lithium Sulfate at High Pressures

A. K. Mishra,[†] Chitra Murli,*[,†] Ashok K. Verma,[†] Yang Song,[‡] M. R. Suresh Kumar,[§] and Surinder M. Sharma[†]

[†]High Pressure & Synchrotron Radiation Physics Division, Bhabha Atomic Research Centre, Mumbai-400085, India

[‡]Department of Chemistry, University of Western Ontario, London, Ontario N6A 5B7, Canada

[§]Department of Physics, Dr. M. V. Shetty Institute of Technology, Mangalore 574225, India

ABSTRACT: The conformation of glycine has been a subject of extensive research for the past several years. As glycine exists in zwitterionic form in liquids and solids, the experimental observations of its neutral conformation are very limited. The complexes of glycine are simple prototypes to study the conformational properties of glycine. We have investigated the high-pressure behavior of glycine lithium sulfate (GLS), a semiorganic complex of glycine using X-ray diffraction, Raman spectroscopy, and density functional theory (DFT)-based first principles calculations. Our Raman studies and DFT calculations suggest formation of an intramolecular hydrogen bond at higher pressures. Subsequent to a structural transformation to a new high-pressure phase at ∼9 GPa, the observed spectral changes in the Raman spectra above 14 GPa indicate possible conformational change of glycine from zwitterionic to neutral form. At pressures above 18 GPa, the characteristic features in the Raman spectra and the X-ray diffraction patterns suggest transformation to a hydrogen-bond-assisted polymeric phase with intermediate range order.

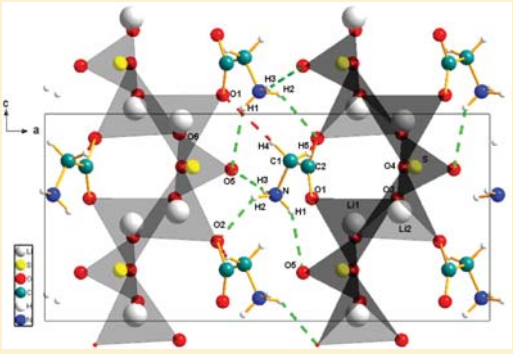

1. INTRODUCTION

Glycine, the simplest amino acid, due to its conformational flexibility, is often found in the folds of proteins, where other amino acids cannot be easily accommodated. The conformational properties of glycine have therefore been studied extensively by theoretical and experimental methods for several years.[1−7] Glycine is known to exist in neutral conformation in the gaseous phase, while it is zwitterionic in solids and aqueous solutions. As a result, experimental observations of neutral conformation of glycine (NH_2CH_2COOH), which is in gaseous phase or as clusters, are limited.[5,6] In the case of complexes, there are large number of organic and inorganic solid complexes of glycine with different conformations such as the zwitterionic ($NH_3^+CH_2COO^-$), cationic ($NH_3^+CH_2COOH$), and anionic ($NH_2CH_2COO^-$) forms,[8−14] among which only a few complexes are known to exist in neutral form.[15−17] Under compression, when molecules are brought closer beyond the steric limits, repulsive forces necessitate the reorientation or rearrangement of molecular units in a material resulting in new crystal structures.[18] Hence, by investigating various glycine complexes under pressure, one can explore its conformational states, which are otherwise not accessible under ambient conditions. High-pressure investigations of these complexes can therefore be of relevance to biomedical and material research applications.

The glycine complexes have also attracted much interest due to their prospective applications as nonlinear optical materials.[10−14] As the structure and properties of glycine and its complexes are governed by hydrogen bonds, high-pressure studies of these interactions are also of importance from the point of view of advanced material research applications.[19,20] Hydrogen-bonded materials are known to undergo pressure-induced structural changes[21−27] through rearrangement,[28−31] reconstruction,[32−34] and symmetrization of hydrogen bonds,[35,36] proton disorder,[37,38] conformational changes,[39] and hydrogen-bond-assisted polymerization.[38] Glycine lithium sulfate, [$(C_2H_5NO_2)$ (Li_2SO_4)], a semiorganic complex of glycine, is a nonlinear optical material, and its structural, mechanical, and optical properties are well studied.[40−42] At ambient conditions, it crystallizes in the orthorhombic structure with $Pna2_1$ space group with four formula units per unit cell and with lattice parameters a = 16.423 Å, b = 5.005 Å, c = 7.654 Å.[40] The structure of GLS constitutes corrugated sheets of [LiO_4] and [SO_4] tetrahedra as seen along [001] as shown in Figure 1. These sheets consist of three crystallographically different tetrahedra (around Li1, Li2, and S atoms), which are corner linked. The non shared vertex of each tetrahedron faces away from the sheets. Consequently, the glycine molecules ($NH_3^+CH_2COO^-$) are located in the interstices and are connected to the sheets through N−H···O hydrogen bonds whose bond distances and angles are N···O5 = 2.868 Å, H3···O5 = 2.07 Å, ∠N−H3···O5 = 160°, N···O2 = 2.816 Å,

Received: April 23, 2013
Revised: June 21, 2013
Published: June 24, 2013

   dx.doi.org/10.1021/jp404017r | J. Phys. Chem. A 2013, 117, 5734−5741

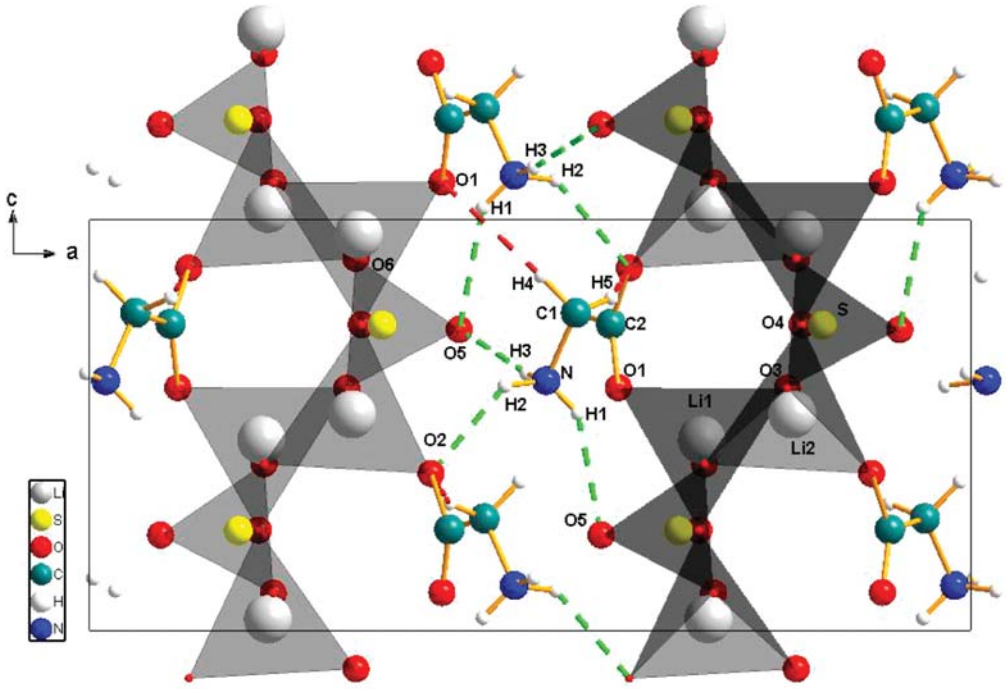

Figure 1. Crystal structure (space group, $Pna2_1$) of glycine lithium sulfate as seen along [010]; dotted lines show N−H···O bonds (green) and C−H···O bonds (red).

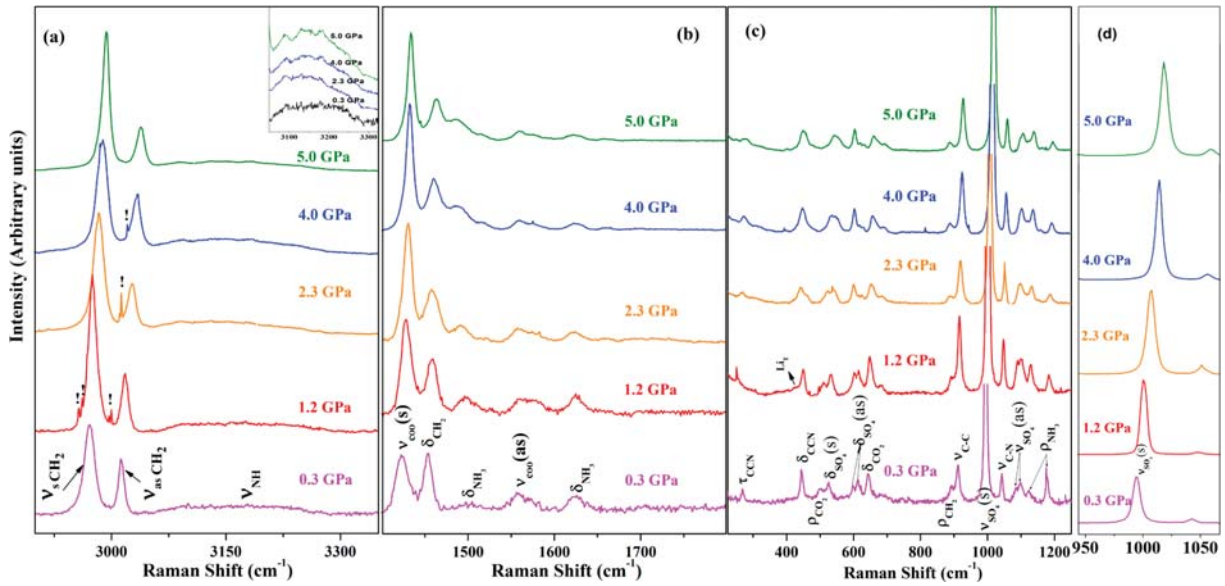

Figure 2. Raman spectra of GLS in the pressure range 0.3−5 GPa in the spectral region: (a) 2900−3350 cm^{-1}; "!" indicate spurious peaks; inset shows weak spectral features modulating the N−H stretching band; (b) 1400−1800 cm^{-1}; (c) 225−1250 cm^{-1}; and (d) 940−1075 cm^{-1}.

H2···O2 = 2.14 Å, ∠N−H2···O2 = 130°, N···O5 = 3.066 Å, H1···O5 = 2.32 Å, and ∠N−H1···O5 = 147°. In addition, the C−H···O distances, that is, C1···O2 = 3.320 Å, H5···O2 = 2.533 Å, ∠C1−H5···O2 = 141.539°; C1···O1 = 3.501 Å, H4···O1 = 2.55 Å, and ∠C1−H4···O1 = 176.627°, are also very close to form hydrogen bonds. Compression of corrugated sheets of LiO_4 and SO_4 tetrahedra in GLS can have a profound effect on the intermolecular hydrogen-bonding interactions, which connect these sheets to the glycine molecules and result in new high-pressure phases. We have carried out high-pressure Raman scattering, X-ray diffraction, and density function theory-based calculations to investigate the nature of structural variations in this compound under pressure. We report here substantial changes in the hydrogen-bonding interactions leading to a change in the conformational state of glycine in GLS at ∼14 GPa and subsequent hydrogen-bond-assisted polymerization at higher pressures.

2. METHODS

Glycine lithium sulfate crystals were grown by slow evaporation of aqueous solution of glycine and lithium sulfate taken in 1:1

dx.doi.org/10.1021/jp404017r | J. Phys. Chem. A 2013, 117, 5734−5741

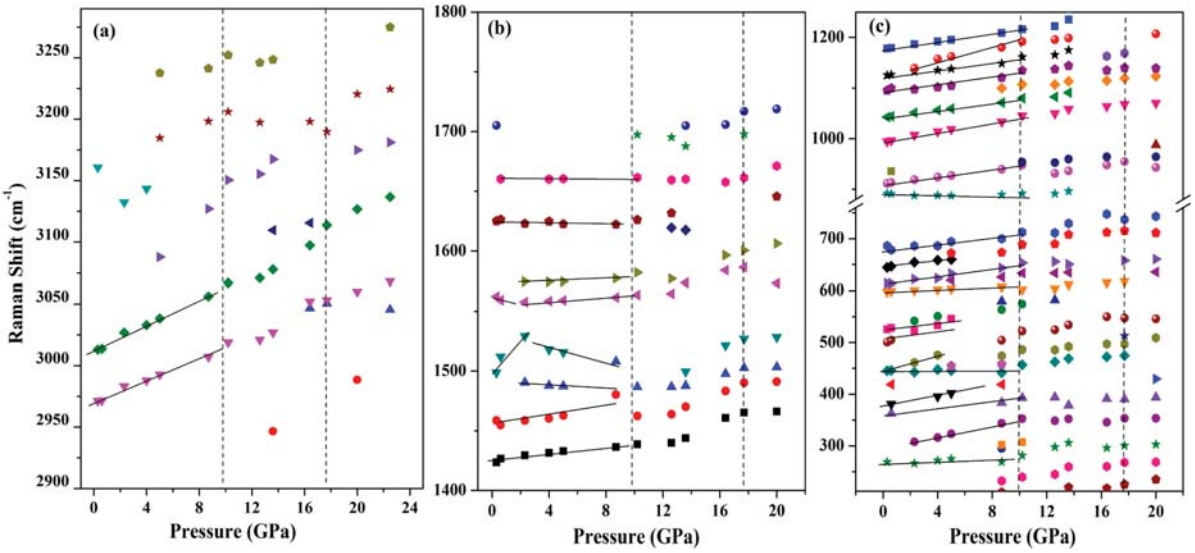

Figure 3. Pressure-induced variation of Raman shifts in the spectral region: (a) 2900−3300 cm^{-1}; (b) 1400−1800 cm^{-1}; and (c) 225−1250 cm^{-1}.

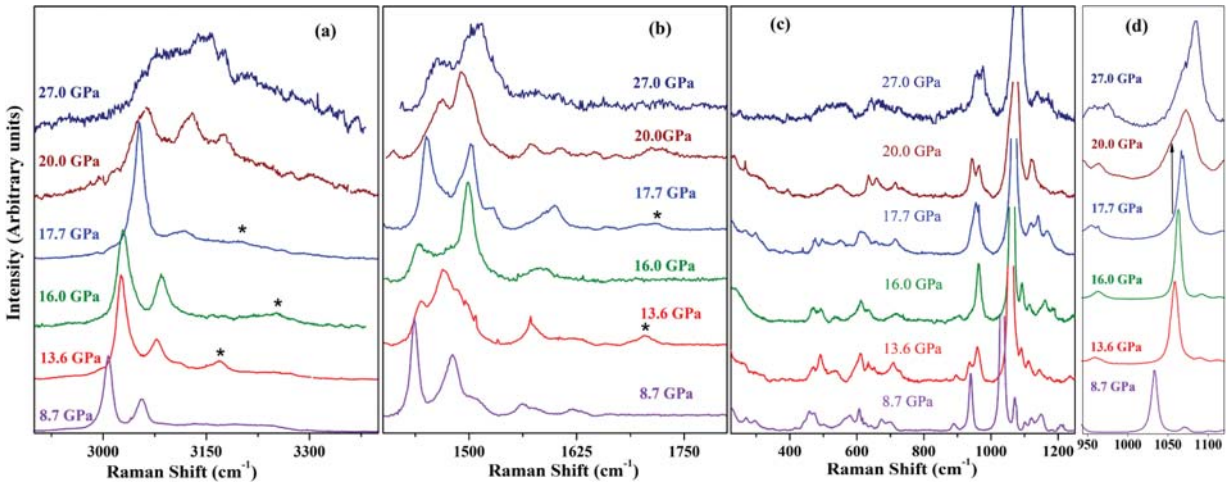

Figure 4. Raman spectra of GLS in the pressure range 8.7−27 GPa in the spectral region: (a) 2900−3350 cm^{-1}; (b) 1400−1800 cm^{-1}; (c) 225−1250 cm^{-1}; and (d) 940−1150 cm^{-1}; "*" denotes new Raman modes.

molar ratio.[41] Polycrystalline samples were loaded along with a ruby chip in a hole of size ∼100 μm in the center of a tungsten gasket preindented to a thickness of 70 μm in a Mao-Bell type of diamond anvil cell. A diode pumped solid state (DPSS) Nd:YAG laser with wavelength 532 nm was used as an excitation source. Edge filter was used to eliminate the Rayleigh line. High-pressure Raman spectra were recorded using our indigenous confocal micro Raman setup, which is built around a single stage Jobin-Yvon HR 460 spectrograph with a liquid N_2 cooled Spectrum-One CCD detector. High-pressure angle dispersive powder X-ray diffraction (ADXRD) experiments were carried out using synchrotron radiation at HPCAT 16, Advanced Photon Source with monochromatic wavelength 0.3680 Å. Pressure measurements employed standard Ruby fluorescence lines.[43] The pressure-induced changes in glycine are very similar under quasi-hydrostatic and nonhydrostatic conditions in the low pressure range.[28] Li_2SO_4 is also a relatively soft inorganic material. To avoid any interaction of the sample with the medium, experiments were performed under non hydrostatic conditions without any pressure transmitting medium. The first-principles structural relaxations, as a function of volume, were carried out using VASP computer code[44−47] with Perdew−Burke−Ernzerhof exchange correlation.[48] The interactions between valence electrons and core were treated within the frozen-core all electron projector-augmented-wave (PAW) approach. Plane wave basis set was constructed using an 800 eV energy cutoff, and the full Brillouin zone was sampled using 2 × 8 × 8 Monkhorst−Pack **k** point meshes.[49]

3. RESULTS AND DISCUSSION

3.1. Raman Spectroscopic Investigations. Raman spectra of GLS have been recorded at different pressures up to 27 GPa. All of the observed spectral changes in the spectral region 200−3400 cm^{-1} have been presented excluding 1300−1400 cm^{-1} where an intense Raman peak of diamond appears. The observed Raman modes are assigned on the basis of earlier work on glycine[28] and lithium sulfate,[50,51] and these assignments are shown in their respective plots in Figure 2, which

dx.doi.org/10.1021/jp404017r | J. Phys. Chem. A 2013, 117, 5734−5741

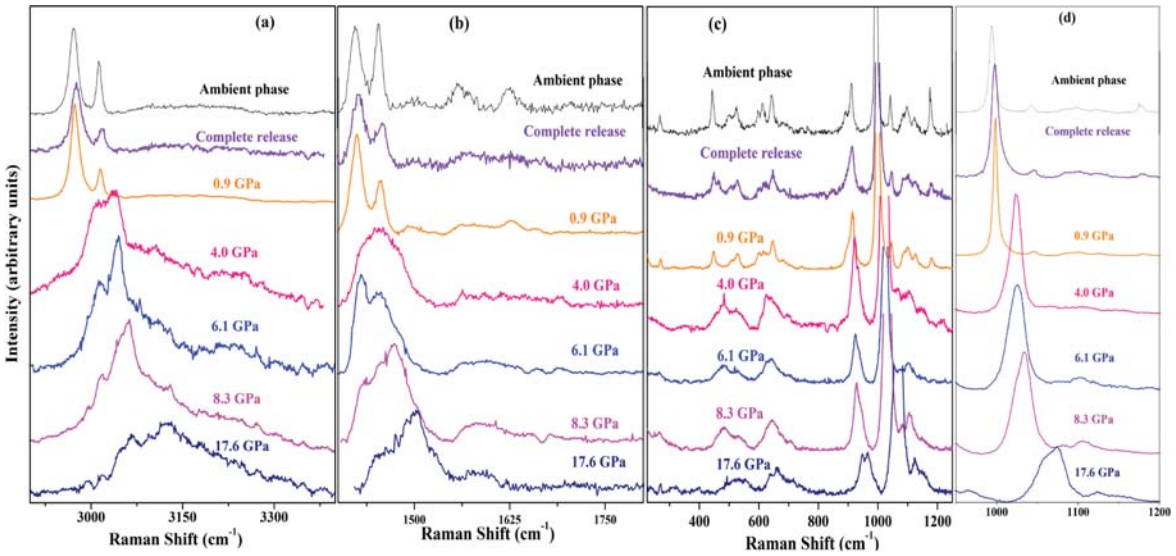

Figure 5. Raman spectra of GLS under decompression in pressure range 27 GPa to 0.1 MPa in the spectral region: (a) 2900−3350 cm^{-1}; (b) 1400−1800 cm^{-1}; (c) 225−1250 cm^{-1}; and (d) 950−1200 cm^{-1}.

displays Raman spectra of GLS recorded in close intervals in the pressure range from 0.3 GPa to 5.0 GPa.

3.2. Spectral Changes below 8.7 GPa. As shown in Figure 2, NH stretching mode is observed as a very broad band with an approximate peak position at ∼3161 cm^{-1}. At pressures above 2.3 GPa, very weak but relatively sharper spectral features appear over the broad N−H band as shown in the inset of Figure 2a. The repeatability of these features in different experiments indicates that these peaks are not statistical fluctuations. Pressure-induced variations of Raman shifts are given in Figure 3. Most of the observed modes such as CH_2 symmetric (2972 cm^{-1}) and antisymmetric (3013 cm^{-1}) stretch, CO_2 antisymmetric stretch (1562 cm^{-1}), CH_2 scissor (1456 cm^{-1}), CO_2 symmetric stretch (∼1425 cm^{-1}), NH_3 rock (1125 and 1178 cm^{-1}), C−N stretch (∼1044 cm^{-1}), SO_4 symmetric stretch (∼996 cm^{-1}), C−C stretch (913 cm^{-1}), CO_2 bend (∼645 cm^{-1}), CO_2 rock (∼500 cm^{-1}), and the CC torsion (∼268 cm^{-1}) blue shift with pressure, and some of the modes such as CH_2 rock (892 cm^{-1}), NH_3 deformation (1500 cm^{-1}) red shift with pressure.

3.3. Spectral Changes above 8.7 GPa. The Raman spectra in the pressure range 8.7−27 GPa are shown in Figure 4. At 13.6 GPa, two new well-resolved modes emerge at ∼1700 cm^{-1} near the C═O region and ∼3170 cm^{-1} near the N−H stretch band, which are marked as an asterisk (*). These two modes show nonmonotonic and anomalous behavior in the pressure range 13.6−17.7 GPa. At 16 GPa when the mode around 3170 cm^{-1} in the NH band blue-shifted (stiffen) to 3180 cm^{-1}, the new mode that appeared at ∼1700 cm^{-1} in the C═O spectral region disappeared. However, at 17.7 GPa, when the new mode of NH band showed softening, the new mode adjacent to 1700 cm^{-1} reappeared and split at further higher pressures. The CH_2 stretching modes continue to blue shift with pressure as shown in Figure 4a. Other spectral changes that are noted across 13.6 GPa are splitting of C−C and SO_4 stretch mode, CN stretch mode, and softening of CH_2 rocking mode as shown in Figure 4c. There are also nonmonotonic changes noted in the position and the relative intensities of the C−C and SO_4 stretch, CO_2 symmetric stretch, and CH_2 scissor modes. At 17.7 GPa, several new bands are observed in the spectral region 1400−1850 cm^{-1} as shown in Figure 4b. At 20 GPa, the relative intensity of the CH_2 symmetric stretch with respect to the other CH_2 and NH_2 stretching modes reduces considerably, and new modes emerge as a shoulder to both the CH_2 symmetric and the antisymmetric stretching modes. Above this pressure, CH_2 and NH_2 stretching modes are seen riding over a broad band. CH_2 stretch continues to blue shift, NH_2 stretching mode softens, and the relative intensity of the CH_2 symmetric stretch with respect to other modes reduces considerably.

The separation between CH_2 symmetric and antisymmetric stretching modes is found to be large (e.g., ∼70 cm^{-1}) at higher pressures as compared to the value of ∼40 cm^{-1} at ambient conditions. A broad band envelops the entire spectral region of CH_2 and NH_2 stretching modes at 27 GPa. The Raman spectra recorded under decompression are shown in Figure 5. On release of pressure, this band is found to persist up to 4 GPa, as shown in Figure 5a, with varied relative intensities of CH_2 and NH_2 stretching modes. However, at 0.9 GPa the spectra observed in this region are very similar to those in the ambient phase, which indicates the reversibility of the observed spectral changes.

3.4. X-ray Diffraction and DFT Calculations. The diffraction pattern at ambient conditions could be indexed to orthorhombic structure with $Pna2_1$ space group. Figure 6 shows the Rietveld refined diffraction pattern of GLS at ambient conditions. Lattice parameters of GLS at ambient conditions deduced from Rietveld refinement of the powder diffraction profile are a = 16.468(2) Å, b = 5.009(1) Å, c = 7.659(3) Å, which are in close agreement with the earlier reported values.[40] The goodness of fit parameters are R_p = 13%, R_{wp} = 16%, with R_F^2 = 21%. The difference in the intensities of the XRD peaks is because the powder XRD data have been collected inside DAC with limited angular range, and the preferred orientation of the crystallites makes it difficult to exactly match with the observed data. The lattice parameters obtained from DFT calculations are a = 16.842 Å, b = 5.062 Å, c = 7.738 Å leading to a slightly expanded cell volume (∼4.6%) as compared to experimental data. Figure 7 shows the angle dispersive X-ray diffraction

dx.doi.org/10.1021/jp404017r | J. Phys. Chem. A 2013, 117, 5734−5741

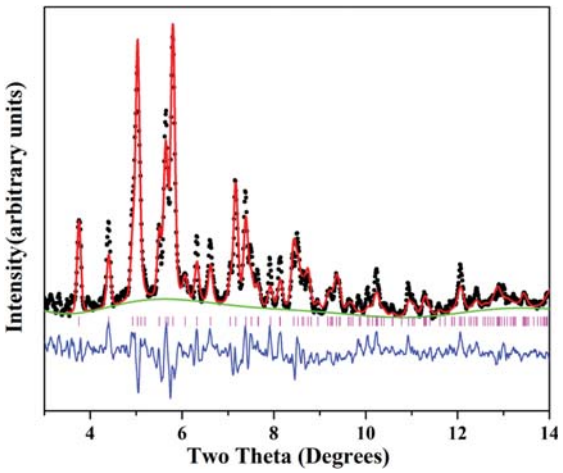

Figure 6. Rietveld refinement of GLS at ambient conditions in *Pna*21 space group. Black circles represent the observed diffraction data; red, green, and blue colored solid lines correspond to calculated diffraction pattern, background, and difference between the observed and calculated intensities, respectively (color online).

patterns of a powdered sample of GLS at a few representative pressures in the pressure range from 0.1 MPa to 21 GPa.

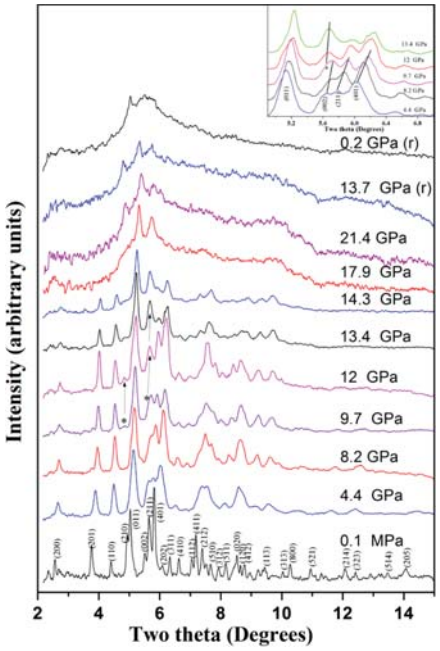

Figure 7. Diffraction patterns of GLS stacked at a few representative pressures; "*" indicates new XRD peaks. Inset shows the magnified diffraction patterns at a few pressures in the region 4.9−7°.

3.5. High-Pressure Phases of GLS. At pressures up to 5 GPa, we observed shifting of all of the diffraction peaks toward higher angular values and redistribution of intensity among X-ray diffrcation peaks. We have determined the lattice parameters of GLS at high pressures through Le Bail analysis[52] of the observed XRD data. Pressure-induced variation of lattice parameters, as given in Figure 8i, shows that compression along the "*a*" axis is more as compared to those along the "*b*" and "*c*" axes. This trend is reproduced by theoretical calculations extremely well. Figure 8j shows the pressure-induced variation of lattice strains in the directions of principal axes. As for the orthorhombic crystal system, the principal axes of strain tensor coincide with crystallographic axes; the linear strain[21] is defined as $\varepsilon_i = \Delta L/L = (a_{ip} - a_{iamb})/a_{iamb}$, where a_{iamb} is lattice parameters at ambient conditions and a_{ip} represents the lattice parameters at different pressures. The anisotropy of the lattice strain is evident from this figure, and it establishes the direction of maximum and minimum strain to be along *a* and *b* axes, respectively. The bulk moduli reported for some amino acids are L-alanine [31.5(14) GPa],[53] L-α glutamine [26.0(11) GPa)],[54] serine monohydrate [18.9(3) GPa],[55] L-cysteine [29.1(4)] GPa,[56] and bis (glycinium) oxalate [35.7(1.1) GPa],[33] whereas the bulk modulus of Li_2SO_4 is ∼54 GPa.[57] The observed pressure−volume data of GLS up to ∼10 GPa are also fitted with third-order Birch−Murnaghan equation of state as shown in Figure 8k, and the bulk modulus determined from the experimental data points is $B_0 \approx 51.3 \pm 16.8$ GPa with its pressure derivative fixed as 4, and the large error is because of less number of available data points. The bulk modulus obtained from DFT calculations is ∼33.6 GPa. The higher rate of compression along the *a* axis implies considerable compression of corrugated sheets of the constituent polyhedra, which would lead to sterical congestion and necessitate structural changes through the reorientation/rearrangement of the molecular units.[18] The reorientation of the LiO_4 and SO_4 tetrahedra is known to be the easy form of deformation in these corner-linked tetrahedral compounds. The corner-sharing tetrahedra in the polymorphs of $LiASO_4$ (A = K, Rb, Cs, etc.) have been found to become edge-sharing tetrahedra at higher pressures.[58] As shown in Figure 7, on further raising the pressure of GLS to ∼9.7 GPa, two new X-ray diffraction peaks appear at 2θ = 4.88° (adjacent to (d_{110})) and 2θ = 5.63° (adjacent to 002 peak), which indicate that there is a structural transformation to a new high-pressure phase II across this pressure. The new peak at 2θ = 5.63° is well resolved at higher pressures as seen in the inset of Figure 7, where zoomed in views of diffraction patterns are given for the pressure range 8.2−14 GPa. To determine the crystal structure of the new high-pressure phase at 9.3 GPa, we tried to index the observed XRD peaks using Crysfire package,[59] but data are not sufficient for the structural refinement. At further higher pressures ∼17.9 GPa, as one can see from Figure 7, the observed diffraction pattern evolves into two broad humps, having two remnant peaks riding over the first hump. The X-ray diffraction peaks generally show broadening under pressure due to inhomogeneous stress distribution in a sample loaded in the gasket hole under nonhydrostatic conditions. However, the appearance of two broad bands on which the individual broad diffraction peaks ride over at pressures ∼17 GPa can be clearly distinguished as due to the emergence of polymeric phase. These observations therefore indicate a structural phase transition across this pressure.

3.6. Zwitterionic to Neutral Form of Glycine in GLS. In the ambient phase of GLS, glycine molecules are located in the interstices between the corrugated sheets formed by LiO_4 and SO_4 tetrahedra. As these sheets are connected to the glycine molecules through hydrogen bonds, there can be considerable changes in the inter- and intramolecular hydrogen bonds under pressure. One can see from the inset of Figure 2 that weak and relatively sharp spectral features appear and modulate the NH stretching band in the pressure range 0.3−5 GPa. The profiles of the OH/NH spectral bands are sensitive to the presence of intramolecular hydrogen bonds, the linearity of the intermo-

dx.doi.org/10.1021/jp404017r | J. Phys. Chem. A 2013, 117, 5734−5741

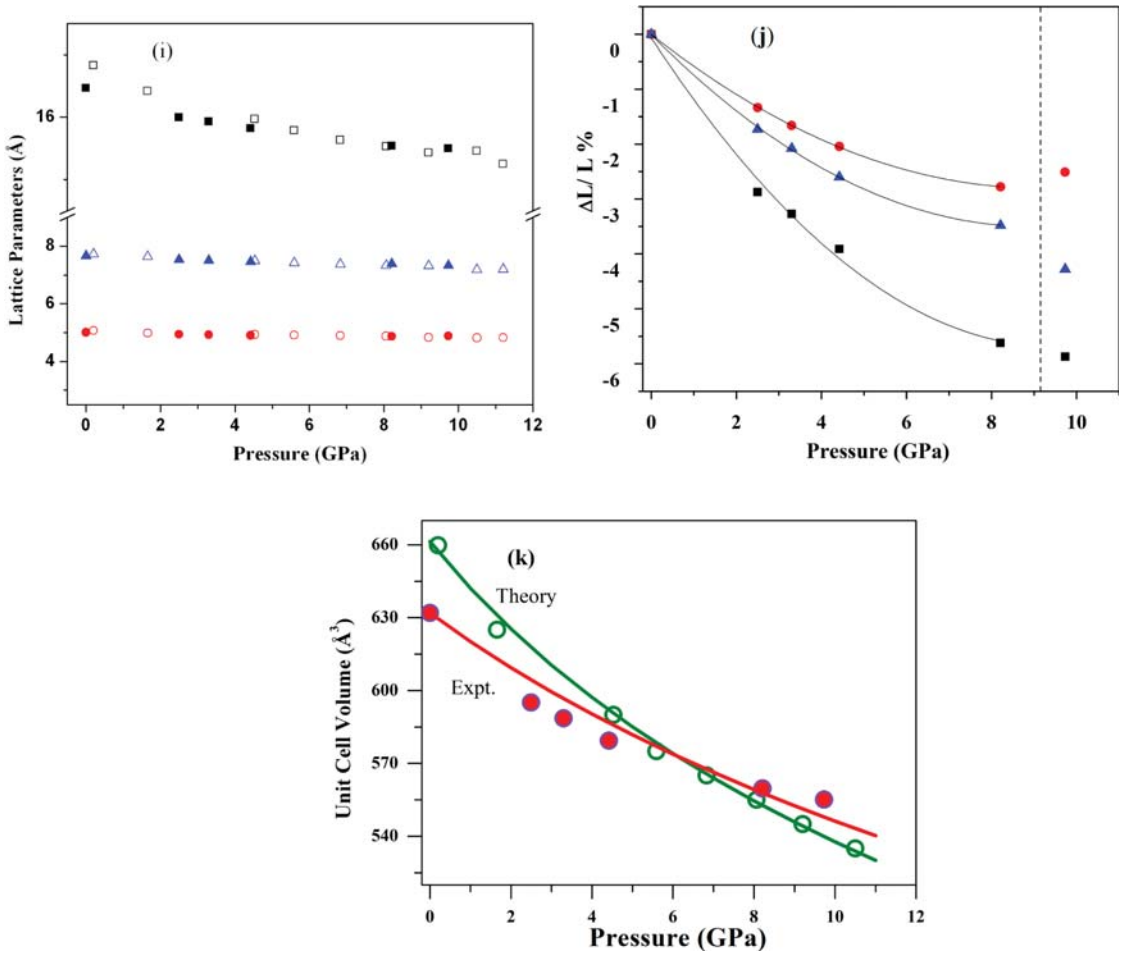

Figure 8. Pressure-induced variation of (i) lattice parameters; square, circle, and triangle symbols represent *a*, *b*, and *c*; (j) lattice strain in the direction of principal axes; (k) V/V_0 of GLS; lines represent second-order BM equation of state fit to pressure-volume data; filled symbols represent the experimental data, and open symbols represent theoretical data.

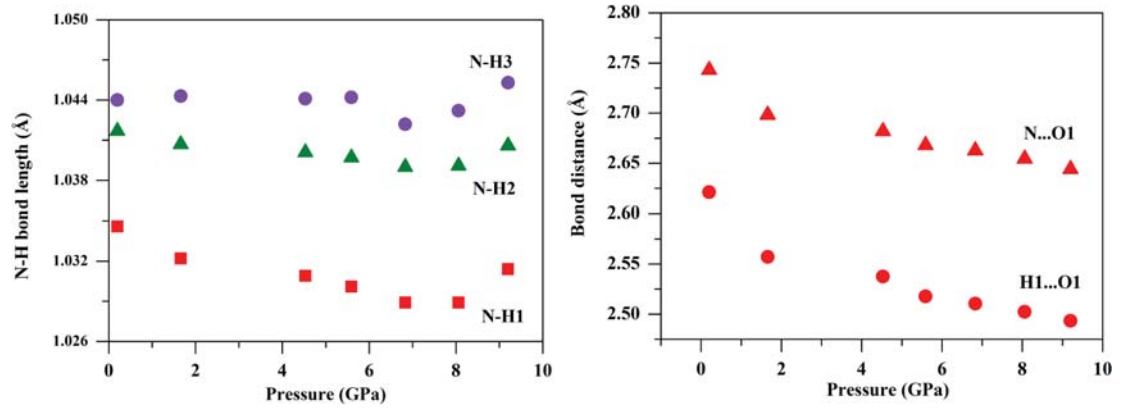

Figure 9. Variation of calculated bond lengths of GLS with pressure. Intramolecular hydrogen-bond parameters are shown in red color (color online). There is an offset in the ambient theoretical bond parameters with respect to the reported values.[27]

lecular hydrogen bonds, and the chemical environment.[37,60,61] It may be noted that in the ambient phase of GLS, in addition to the three N−H···O intermolecular hydrogen bonds, the intramolecular N−H1···O1 distance (N···O1= 2.669 Å; H1···O1 = 2.422 Å) is also quite close to hydrogen-bond formation.[40] The strengthening of this intramolecular hydogen bond N1−H1···O1 under pressure can lead to change in its ionic nature, that is, from zwitterionic glycine to a neutral glycine at high pressures. Our Raman spectroscopic observations of GLS indicate such a possibility due to the following reasons.

The neutral form of glycine has an NH_2 molecular unit, which gives rise to a relatively stronger Raman mode as compared to the weak and broader Raman mode arising from

dx.doi.org/10.1021/jp404017r | J. Phys. Chem. A 2013, 117, 5734−5741

the NH_3 molecular unit of zwitterionic glycine.[62] As one can see from Figure 4a, at 13.6 GPa, a well-resolved peak, which may be assoicated with the NH_2 stretching mode, emerges at ~3170 cm^{-1} riding over the broad NH band. This is also accompanied by the appearance of a well-resolved peak (~1700 cm^{-1}) in the C═O stretching region. The appearance of the C═O stretch mode indicates that the NH_3 molecular unit is deprotonated. The observed spectral features indeed closely resemble the Raman spectra of a neutral form of glycine.[9,63] However, the vibrational properties and assignments are dependent on the particular conformation of the neutral form.[9,64] The structural details of the high-pressure phase would be required to give a complete account of the observed vibrational features in this high-pressure phase. To search for the possible signature of intramolecular hydrogen bond and changes in the conformation, we have also carried out full structural relaxation of the unit cell as a function of pressure using ab initio calculations. As one can see from Figure 9, the intramolecular (N1)H1···O1 distance shows a decreasing trend. This is consistent with the suggestion that the strength of this hydrogen bond increases at higher pressures. It is also inferred from the DFT calculations that the interlayer C−H---O hydrogen-bond distances show a decreasing trend with pressure. Also, the reduction in the C−H covalent bond length suggests the formation of blue-shifting C−H---O hydrogen bonds at high pressures.

At pressures above 9 GPa, if this intramolecular N−H1···O1 hydrogen bond is further strengthened along with the reorientations of the other molecular units in the high-pressure phase II, the formation of the neutral form of glycine may be possible. Also, a large increase in the separation between peak positions of CH_2 symmetric and antisymmetric stretching modes, which are reported to be assoicated with a change in the planar to bent geometry,[65] suggests that there are indeed substantial changes in the orientations of submolecular units of GLS. High-pressure neutron diffraction studies would be very useful to determine the hydrogen-bond parameters at high pressures and confirm the possibilities suggested by our investigations. In addition, there are nonmonotonic and anomalous changes observed in the Raman spectra in the pressure range 13.6−17.7 GPa. Similar anomalous spectral changes observed in formic acid under pressure have been attributed to vibrational mode coupling.[38] In the case of GLS, the observed nonmonotonic changes in the spectra may be due to the intrinsic changes in the structural parameters under pressure.

3.7. Hydrogen-Bond-Assisted Polymerization at ~18 GPa. The change from the zwitterionic to neutral form of glycine would involve deprotonation of NH_3 unit and consequent changes in the electronic state of carboxyl group, which would strengthen the intersheet N−H2···O2 or C1−H5···O2 hydrogen-bonding interactions under further compression. Above 17.7 GPa, the splitting and drastic reduction in the relative intensity of CH_2 symmetric stretching mode, the softening of the NH_2 stretching mode, and appearance of a broad band in the region of the CH_2 and NH_2 stretch modes accompanied by drastic changes in several other modes suggest structural transformation to a C−H···O/N−H···O hydrogen-bond-assisted polymeric phase III. The disappearance of most of the XRD peaks and appearance of the broad bands above ~18 GPa suggest loss of long-range order in phase III. The emergence of two broad diffraction humps, which could be viewed as the first and second sharp diffraction peaks corresponding to a noncrystalline polymeric phase,[66] indicates intermediate range order resulting from the correlations between main corrugated chains. On release of pressure, both X-ray diffraction patterns and Raman spectra showed large hysteresis. While the Raman spectra on decompression at 0.9 GPa resemble the ambient spectra, X-ray diffraction patterns indicate the persistence of the disordered phase even up to 0.2 GPa. However, the observed Raman spectra on complete release reveal that polymerization, which is mediated through noncovalent interaction, that is, hydrogen-bonding interaction, is completely reversible, implying this high-pressure phase to be a reversible polymeric phase.

4. CONCLUSIONS

Our high-pressure X-ray diffraction, Raman scattering, and first principles density functional theory-based structural relaxation calculations of glycine lithium sulfate indicate structural transformations to new high-pressure phases, which can be of importance to advanced material research applications. A structural transformation to a new phase II at ~9 GPa along with the strengthening of an intramolecular hydrogen bond of glycine in GLS is indicated by our high-pressure investigations. The spectral changes across ~14 GPa suggest possibile changes in the conformational state of glycine from zwitterionic to neutral form. At further higher pressures above 18 GPa, the broad spectral features in the Raman spectra and the emergence of two broad diffraction humps indicate transformation to a hydrogen-bond-assisted polymeric phase III with an intermediate range order. The observed pressure-induced structural changes are completely reversible on release from 26 GPa. The observation of conformational changes of glycine in this semiorganic complex at high pressures suggests that glycine complexes can be model systems to study the conformational flexibility of glycine and can be of relevance to biomedical and material research applications.

AUTHOR INFORMATION

Corresponding Author

*Tel.: 91-22-25591326. Fax: 91-22-25595296. E-mail: cmurli@barc.gov.in.

Notes

The authors declare no competing financial interest.

ACKNOWLEDGMENTS

High-pressure X-ray diffraction data were collected at HPCAT (Sector 16), Advanced Photon Source (APS), Argonne National Laboratory. HPCAT operations are supported by DOE-NNSA under Award No. DE-NA0001974 and DOE-BES under Award No. DE-FG02-99ER45775, with partial instrumentation funding by NSF. APS is supported by DOE-BES, under Contract No. DE-AC02-06CH11357. We acknowledge the technical assistance provided by Dr. Y. Meng for the X-ray diffraction experiments. C.M. and S.M.S. are thankful to Dr. S. K. Sikka for his valuable suggestions and discussions. C.M. acknowledges the Centre for Chemical Physics (CCP) Fellowship from the University of Western Ontario. Y.S. acknowledges the Natural Science and Engineering Research Council of Canada for Discovery Grants.

REFERENCES

(1) Csăszăr, A. G. *J. Am. Chem. Soc.* **1992**, *114*, 9568−9575.

(2) Hu, C. H.; Shen, M.; Schaefer, H. F., III. *J. Am. Chem. Soc.* **1993**, *115*, 2923−2929.
(3) Sirois, S.; Proynov, E. I.; Nguyen, D. T.; Salahub, D. R. *J. Chem. Phys.* **1997**, *107*, 6770−6781.
(4) Tse, Y. C.; Newton, M. D.; Vishveshwara, S.; Pople, J. A. *J. Am. Chem. Soc.* **1978**, *100*, 4329−4331.
(5) Vijay, A.; Sathyanarayana, D. N. *J. Phys. Chem.* **1992**, *96*, 10735−10739.
(6) Huisken, F.; Werhahn, O.; Ivanov, A. Yu.; Krasnokupski, S. A. *J. Chem. Phys.* **1999**, *111*, 2978−2984.
(7) Balabin, R. M. *J. Phys. Chem. Lett.* **2010**, *1*, 20−23.
(8) Fleck, M. *Z. Kristallogr.* **2008**, *223*, 222−232.
(9) Rosado, M. T.; Duarte, M. L. T. S.; Fausto, R. *Vib. Spectrosc.* **1998**, *16*, 35−54 and references therein.
(10) Pepinsky, R.; Okaya, Y.; Eastman, D. P.; Mistui, T. *Phys. Rev.* **1957**, *107*, 1538−1539.
(11) Pepinsky, R.; Vedam, K.; Hoshino, S.; Okaya, Y. *Phys. Rev.* **1958**, *111*, 430−432.
(12) Santra, L.; Verma, A. L.; Bajpai, P. K.; Hilczer, B.; Huong, P. V. *J. Phys. Chem. Solids* **1994**, *55*, 405−411.
(13) Ghazaryan, V. V.; Fleck, M.; Petrosyan, A. M. *J. Mol. Struct.* **2010**, *977*, 117−129.
(14) Choudhary, R. R.; Panicker, L.; Chitra, R.; Sakuntala, T. *Solid State Commun.* **2008**, *145*, 407−412.
(15) Davies, H. O.; Brown, D. A.; Yanovsky, A. I.; Nolan, K. B. *Inorg. Chim. Acta* **1995**, *237*, 71−77.
(16) Losev, A. E.; Zakharov, B. A.; Drebushchak, T. N.; Boldyreva, E. V. *Acta Crystallogr., Sect. C* **2011**, *67*, o297−o300.
(17) Riscob, B.; Shakir, M.; Sundar, J. K.; Natarajan, S.; Wahab, M. A.; Bhagavannarayana, G. *Spectrochim. Acta, Part A* **2011**, *78*, 543−548.
(18) Sharma, S. M.; Sikka, S. K. *Prog. Mater. Sci.* **1996**, *40*, 1−77.
(19) Moulton, B.; Zaworotko, M. J. *Chem. Rev.* **2001**, *101*, 1629−1658.
(20) Wojtecki, R. J.; Meador, M. A.; Rowan, S. J. *Nat. Mater.* **2011**, *10*, 14−27.
(21) Zakharov, B. A.; Boldyreva, E. V. *Acta Crystallogr., Sect. B* **2013**, *69*, 271−280.
(22) Minkov, V. S.; Boldyreva, E. V.; Drebushchak, T. N.; Görbitz, C. H. *CrystEngComm* **2012**, *14*, 5943−5954.
(23) Boldyreva, E. V.; Ivashevskaya, S. N.; Sowa, H.; Ahsbahs, H.; Weber, H. P. *Dokl. Phys. Chem.* **2004**, *396*, 1−4.
(24) Goryainov, S. V.; Kolesnik, E. N.; Boldyreva, E. V. *Physica B* **2005**, *357*, 340−347.
(25) Boldyreva, E. V. *Phase Transitions* **2009**, *82*, 303−321 and references therein.
(26) Sikka, S. K.; Sharma, Surinder, M. *Phase Transitions* **2008**, *81*, 907−934.
(27) Boldyreva, E. V. *Acta Crystallogr., Sect. A* **2008**, *64*, 218−231.
(28) Murli, C.; Sharma, S. M.; Karmakar, S.; Sikka, S. K. *Physica B* **2003**, *339*, 23−30.
(29) Kolesnik, E. N.; Goryainov, S. V.; Boldyreva, E. V. *Dokl. Phys. Chem.* **2005**, *404*, 169−172.
(30) Zakharov, B. A.; Losev, E. A.; Boldyreva, E. V. *CrystEngComm* **2013**, *15*, 1693−1697.
(31) Zakharov, B. A.; Losev, E. A.; Kolesov, B. A.; Drebushchak, V. A.; Boldyreva, E. V. *Acta Crystallogr., Sect. B* **2012**, *68*, 287−296.
(32) Mishra, A. K.; Murli, C.; Sharma, S. M. *J. Phys. Chem. B* **2008**, *112*, 15867−15874.
(33) Mishra, A. K.; Murli, C.; Garg, N.; Chitra, R.; Sharma, S. M. *J. Phys. Chem. B* **2010**, *114*, 17084−17091.
(34) Gajda, R.; Katrusiak, A. *Cryst. Growth Des.* **2011**, *11*, 4768−4774.
(35) Aoki, K.; Yamawaki, H.; Sakashita, M.; Fujihisa, H. *Phys. Rev. B* **1996**, *54*, 15673−15677.
(36) Benoit, M.; Marx, D.; Parrinello, M. *Nature* **1998**, *392*, 258−261.
(37) Szafranski, M.; Katrusiak, A.; McIntyre, G. J. *Cryst. Growth Des.* **2010**, *10*, 4334−4338.
(38) Goncharov, A. F.; Manaa, M. R.; Zaug, J. M.; Gee, R. H.; Fried, L. E.; Montgomery, W. B. *Phys. Rev. Lett.* **2005**, *94*, 065505−065508.
(39) Murli, C.; Lu, N.; Dong, Z.; Song, Y. *J. Phys. Chem. B* **2012**, *116*, 12574−12580.
(40) Fleck, M.; Bohaty, L. *Cryst. Struct. Commun.* **2004**, *C60*, m291−m295.
(41) Kumar, S. M. R.; Ravindra, H. J.; Dharmaprakash, S. M. *J. Cryst. Growth* **2007**, *306*, 361−365.
(42) Suresh, S.; Ramanand, A.; Jayaraman, D.; Navis Priya, S. M. *J. Minerals Charact. Eng.* **2010**, *9*, 107−1080.
(43) Piermarini, G. J.; Block, S.; Barnett, J. P.; Forman, R. A. *J. Appl. Phys.* **1975**, *46*, 2774−2780.
(44) Kresse, G.; Hafner, J. *J. Phys.: Condens. Matter* **1994**, *6*, 8245−8257.
(45) Kresse, G.; Furthmuller, J. *Comput. Mater. Sci.* **1996**, *6*, 15−50.
(46) Blochl, P. E. *Phys. Rev. B* **1994**, *50*, 17953−17979.
(47) Kresse, G.; Joubert, D. *Phys. Rev. B* **1999**, *59*, 1758−1775.
(48) Perdew, J. P.; Burke, K.; Ernzerhof, M. *Phys. Rev. Lett.* **1996**, *77*, 3865−3868.
(49) Monkhorst, H. J.; Pack, J. D. *Phys. Rev. B* **1976**, *13*, 5188−5192.
(50) Arora, A. K.; Sakuntala, T. *Solid State Commun.* **1990**, *75*, 855−859.
(51) Sakuntala, T.; Arora, A. K. *J. Phys. Chem. Solids* **2000**, *61*, 103−108.
(52) Larson, A. C.; Von Dreele, R. B. *GSAS: General Structure Analysis System*; Los Alamos National Laboratory: Los Alamos, NM, 2000.
(53) Olsen, J. S.; Gerward, L.; Freire, P. T. C.; Filho, J. M.; Melo, F. E. A.; Filho, A. G. S. *J. Phys. Chem. Solids* **2008**, *69*, 1641−1645.
(54) Casal, P. L.; Allan, D. R.; Parsons, S. *Acta Crystallogr., Sect. B* **2008**, *64*, 466−475.
(55) Johnstone, R. D. L.; Francis, D.; Lennie, A. R.; Marshall, W. G.; Moggach, S. A.; Parsons, S.; Pidcock, E.; Warren, J. E. *CrystEngComm* **2008**, *10*, 1758−1769.
(56) Moggach, S. A.; Allan, D. R.; Parsons, S.; Sawyer, L.; Warren, J. E. *J. Synchrotron Radiat.* **2005**, *12*, 598−607.
(57) Parfitt, D. C.; Keen, D. A.; Hull, S.; Crichton, W. A.; Mezouar, M.; Wilson, M.; Madden, P. A. *Phys. Rev. B* **2005**, *72*, 054121−1−7.
(58) Sankaran, H.; Sikka, S. K.; Sharma, S. M.; Chidambaram, R. *Phys. Rev. B* **1988**, *38*, 170−173.
(59) Shirley, R. *The Crysfire System for Automatic Powder Indexing*; The Lattice: Surrey, UK, 1999.
(60) Tayyari, S. F.; Raissi, H.; Tayyari, F. *Spectochim. Acta, Part A* **2002**, *58*, 1681−1695.
(61) Tan, S. F.; Ana, K. P.; How, G. F. *J. Phys. Org. Chem.* **1991**, *4*, 170−176.
(62) Armstrong, R. S.; Atkinson, I. M.; Carter, E.; Mahinay, M. S.; Skelton, B. W.; Turner, P.; Wei, G.; White, A. H.; Lindoy, L. F. *Proc. Natl. Acad. Sci. U.S.A.* **2002**, *99*, 4987−4992.
(63) Krishnan, R. S.; Balasubramanian, K. *Proc.-Indian Acad. Sci., Sect. A* **1960**, *53*, 105−112.
(64) Ramaniah, L. M.; Chakrabarti, A.; Kshirsagar, R. J.; Kamal, C.; Banerjee, A. *Mol. Phys.* **2011**, *109*, 875−892.
(65) Bykov, S. V.; Myshakina, N. S.; Asher, S. A. *J. Phys. Chem. B* **2008**, *112*, 5803−5812.
(66) Chiba, A.; Funamori, N.; Nakayama, K.; Ohishi, Y.; Bennington, S. M.; Rastogi, S.; Shukla, A.; Tsuji, K.; Takenaka, M. *Phys. Rev. E* **2012**, *85*, 021807−1−5.